

## A QUANTUM SEGMENTATION ALGORITHM BASED ON BACKGROUND-DIFFERENCE METHOD FOR NEQR IMAGE

LU WANG

*School of Information Science and Engineering, Southeast University,  
Nanjing, 211189, China  
Lu.Wang-MT@163.com*

WENJIE LIU\*

*School of Software, Nanjing University of Information Science and Technology,  
Nanjing, 210044, China  
wenjie@163.com*

ZHILIANG DENG

*School of Automation, Nanjing University of Information Science and Technology,  
Nanjing, 210044, China  
mtdzl@163.com*

Received October 30, 2022

Revised November 22, 2023

Quantum image segmentation algorithm can use its quantum mechanism to rapidly segment the objects in a quantum image. However, the existing quantum image segmentation algorithms can only segment static objects in the image and use more quantum resource(qubit). In this paper, a novel quantum segmentation algorithm based on background-difference method for NEQR image is proposed, which can segment dynamic objects in a static scene image by using fewer qubits. In addition, an efficient and feasible quantum absolute value subtractor is designed, which is an exponential improvement over the existing quantum absolute value subtractor. Then, a complete quantum circuit is designed to segment the NEQR image. For a  $2^n \times 2^n$  image with gray-scale range of  $[0, 2^q - 1]$ , the complexity of our algorithm is  $O(q)$ , which has an exponential improvement over the classical segmentation algorithm, and the complexity will not increase as the image's size increases. The experiment is conducted on IBM Q to show the feasibility of our algorithm in the noisy intermediate-scale quantum (NISQ) era.

*Keywords:* Quantum image processing, Quantum image segmentation, Background-difference method, Quantum absolute value subtractor

### 1 Introduction

Currently, our requirements for the image quality are getting higher, which needs more computation to process the images. However, the current development of classic computers is limited by technology, and the real-time problem has gradually emerged. Quantum computing can greatly increase the computation speed due to its unique entanglement and superposition characteristics. Quantum image processing is an interdisciplinary subject that combines classical image processing with quantum computing, which has received extensive attention from researchers in recent years [1]. Quantum image processing utilizes the characteristics

of quantum computing by storing image information in quantum state, which can achieve exponential speed-up than the classical image processing [2].

In quantum image processing, the first is to store classical images in qubits to turn them into quantum images. So, a representation model of quantum images is required. At present, there are two main methods to encode the quantum image. One is to encode the gray-scale values of the quantum image into the probability amplitude of the qubits, which can encode images using fewer qubits, such as qubit lattice representation (QLR) [3], real ket representation (RKR) [4], the flexible representation of quantum image (FRQI) [5], the multi-channel RGB images representation of quantum images (MCQI) [6], a normal arbitrary superposition state of quantum image (NASS) [7] and quantum probability image encoding representation (QPIE) [8]. When an image is retrieved, a large number of measurements are required to get an approximation of the probability magnitude, which makes it difficult to retrieve images. The other method, such as the novel enhanced quantum image representation (NEQR) [9] model, an improved NEQR (INEQR) [10], a generalized model of NEQR (GNEQR) [11], a novel quantum representation of color digital images (NCQI) [12], and quantum representation of multi wavelength images (QRMW) [13], solves this problem well and it is to encode the gray-scale values by using a separate qubit sequence. Because the NEQR model stores the image information in the basic state of the qubit sequence, it is very simple and convenient to operate the pixel directly. In addition, when the quantum image is restored to a classical image, the NEQR model only requires a few measurements. Therefore, the NEQR model is widely used due to its simplicity of operation, and this model is also used in this paper. Based on these representation models, various quantum image processing algorithms have been proposed. The current quantum image processing algorithms mainly include geometrical transformation of quantum image [14], quantum image encryption [15], feature extraction of quantum image [16], quantum image scrambling [17], quantum image morphological operations [18], quantum image watermarking [19], quantum image filtering [20], quantum image edge detection [21, 22, 23, 24], quantum image segmentation [25, 26, 27, 28], etc. Among them, quantum image segmentation is the basis of image processing.

In recent years, quantum image segmentation algorithms have gradually developed from theoretically feasible to practically feasible. In 2014, Caraiman et al. [25] used histograms to segment quantum images. They segmented the image according to the distribution of pixels' gray-scale values in the histogram and obtained exponential acceleration, but there was no specific oracle implementation circuit. One year later, they [26] proposed a quantum image segmentation algorithm based on a single threshold and gave an oracle circuit, but they could not be simulated in the noisy intermediate-scale quantum (NISQ) era due to the high quantum cost. In 2019, Xia et al. [27] designed a quantum comparator and used a single threshold to binarize the quantum image. They designed a detailed segmentation circuit but the complexity is still too high. Although many researchers have conducted research on quantum image segmentation algorithms, but none of the previous algorithms are simulated on the quantum platform. In 2020, Yuan et al. [29] proposed a dual-threshold quantum image segmentation algorithm based on a quantum comparator they designed and simulated it on the IBM Q platform [30], but when the image is more complex, the effect of the segmentation algorithm needs to be improved. The above algorithms can only segment the static objects in the static scene image, and cannot perform effective segmentation when encountering dynamic

objects. In real-world application scenarios, the segmentation of dynamic objects is very extensive, with the most common example being a monitoring system. During a certain period of time, the scene is relatively fixed, but the moving object is constantly changing. So the real-time requirements during the segmentation process are very high. Therefore, a dynamic object segmentation algorithm with high real-time performance is needed. The classic background difference method can quickly and effectively segment dynamic objects under the same background, but with the improvement of image quality, the real-time problem of the algorithm gradually becomes apparent. Therefore, we conducted in-depth research on this issue, and the main contributions are as follows.

- A novel quantum segmentation algorithm based on background-difference method for NEQR image is proposed.
- An efficient quantum absolute value subtractor (QAVS) is designed, and its complexity is exponentially improved compared to the existing absolute value subtractor. Then based on this QAVS, a complete quantum circuit is designed to segment dynamic objects in the static scene image by using few qubits.
- We verify the superiority and feasibility of our proposed algorithm by analyzing the circuit complexity and performing the simulation experiment on IBM Q platform [30] through Qiskit extension[31], respectively.

The rest of this paper is organized as follows: In Sec. 2, the basic quantum gates and the NEQR model are introduced respectively. In Sec. 3, we first introduce the quantum image segmentation algorithm based on background-difference method, and then, a quantum subtractor, a quantum absolute value subtractor and a complete quantum segmentation circuit are designed. In Sec. 4, the circuit complexity is analyzed, and the simulation experiment is conducted on the IBM Q platform to show the feasibility of our algorithm in Sec. 5. Finally, the conclusion is given in Sec. 6. Appendix A gives the complete quantum circuits for the 8-qubit comparator and subtractor.

## 2 Preliminaries



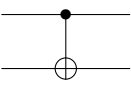
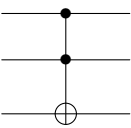
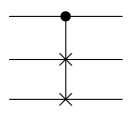
### 2.1 Quantum gates

With the gradual deepening of quantum computing research, there are more and more types of quantum logic gates, and their performance is getting better and better. The optimized quantum logic gate has very low theoretical complexity. However, when operating in an actual quantum circuit, these quantum logic gates need to be combined with a lot of basic quantum logic, which leads to the quantum cost of the actual circuit far exceeding the theoretical cost. Therefore, in this paper, we use basic quantum logic gates to design quantum circuits (i.e., H gate, X gate, CNOT gate, Toffoli gate and Fredkin gate) [32]. The commonly used basic quantum logic gates in quantum computing are shown in Tab. 1.

### 2.2 NEQR

The classical image contains position information and gray-scale value information, and the NEQR model uses three entangled qubit sequences to represent these two kinds of information. Assuming that an image's size is  $2^n \times 2^n$ , and its gray-scale range is  $[0, 2^q - 1]$ . Then, two  $n$ -length qubit sequences are required to represent position information, and  $q$ -length qubit

Table 1. The quantum gates and their unitary matrix.

Quantum gate	Symbol	Unitary matrix
Hadamard gate		$\frac{1}{\sqrt{2}} \begin{bmatrix} 1 & 1 \\ 1 & -1 \end{bmatrix}$
Pali-X gate		$\begin{bmatrix} 0 & 1 \\ 1 & 0 \end{bmatrix}$
CNOT gate		$\begin{bmatrix} 1 & 0 & 0 & 0 \\ 0 & 1 & 0 & 0 \\ 0 & 0 & 0 & 1 \\ 0 & 0 & 1 & 0 \end{bmatrix}$
Toffoli gate		$\begin{bmatrix} 1 & 0 & 0 & 0 & 0 & 0 & 0 & 0 \\ 0 & 1 & 0 & 0 & 0 & 0 & 0 & 0 \\ 0 & 0 & 1 & 0 & 0 & 0 & 0 & 0 \\ 0 & 0 & 0 & 1 & 0 & 0 & 0 & 0 \\ 0 & 0 & 0 & 0 & 1 & 0 & 0 & 0 \\ 0 & 0 & 0 & 0 & 0 & 1 & 0 & 0 \\ 0 & 0 & 0 & 0 & 0 & 0 & 0 & 1 \\ 0 & 0 & 0 & 0 & 0 & 0 & 1 & 0 \end{bmatrix}$
Fredkin gate		$\begin{bmatrix} 1 & 0 & 0 & 0 & 0 & 0 & 0 & 0 \\ 0 & 1 & 0 & 0 & 0 & 0 & 0 & 0 \\ 0 & 0 & 1 & 0 & 0 & 0 & 0 & 0 \\ 0 & 0 & 0 & 1 & 0 & 0 & 0 & 0 \\ 0 & 0 & 0 & 0 & 1 & 0 & 0 & 0 \\ 0 & 0 & 0 & 0 & 0 & 0 & 1 & 0 \\ 0 & 0 & 0 & 0 & 0 & 1 & 0 & 0 \\ 0 & 0 & 0 & 0 & 0 & 0 & 0 & 1 \end{bmatrix}$

sequences are required to represent the gray-scale value information. The NEQR model can be written as Eq. (1) [9].

$$|I\rangle = \frac{1}{2^n} \sum_{Y=0}^{2^n-1} \sum_{X=0}^{2^n-1} |C_{YX}\rangle \otimes |Y\rangle |X\rangle = \frac{1}{2^n} \sum_{YX=0}^{2^{2n}-1} \bigotimes_{k=0}^{q-1} |C_{YX}^k\rangle \otimes |YX\rangle \tag{1}$$

where  $|C_{YX}\rangle = |C_{YX}^{q-1}, C_{YX}^{q-2}, \dots, C_{YX}^1, C_{YX}^0\rangle$  represents the quantum image gray-scale values,  $C_{YX}^k \in \{0, 1\}$ ,  $k = q-1, q-2, \dots, 0$ .  $|YX\rangle = |Y\rangle |X\rangle = |Y_{n-1}, Y_{n-2}, \dots, Y_0\rangle |X_{n-1}, X_{n-2}, \dots, X_0\rangle$  represents the position of the pixel in a quantum image,  $Y_t, X_t \in \{0, 1\}$ .

Fig. 1 shows an example of a grayscale image of size  $2 \times 2$ , and the corresponding NEQR

expression of which is given as follows

$$\begin{aligned}
 |I\rangle &= \frac{1}{2} (|0\rangle |00\rangle + |100\rangle |01\rangle + |200\rangle |10\rangle + |255\rangle |11\rangle) \\
 &= \frac{1}{2} \begin{pmatrix} |00000000\rangle |00\rangle + |01100100\rangle |01\rangle \\ + |11001000\rangle |10\rangle + |11111111\rangle |11\rangle \end{pmatrix} .
 \end{aligned} \tag{2}$$

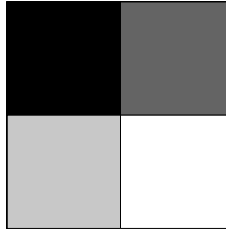


Fig. 1. An example of a  $2 \times 2$  image.

### 3 The quantum image segmentation algorithm and its circuit design

In this section, a quantum image segmentation algorithm based on the background-difference method is proposed. We first introduced the basic idea of the algorithm, and then a series of quantum circuits in the algorithm are designed in detail.

#### 3.1 The quantum image segmentation algorithm

The algorithm can segment the dynamic object in a static scene image, and it performs the subtraction operation between the currently obtained image and the background image, which can obtain the gray-scale image with the object area. In an ideal situation, except for the object area, the gray-scale value of the image we get is 0, so that we can clearly see the object in the image. However, in practical applications, due to the influence of factors such as light changes, the gray-scale value of the obtained gray-scale image will not be 0 except for the object area, which makes it difficult to distinguish the object. Therefore, in order to reduce the influence of these factors as much as possible, we perform a threshold-based binarization process on the gray-scale image after the subtraction processing. When the gray-scale values of the image are greater than the threshold we set, we consider it as the object and set the gray-scale value to 1. Otherwise we consider it to be the background area and set its gray-scale value to 0. From this, we can distinguish the dynamic object in the static scene image well. Fig. 2 represents the workflow of the quantum image segmentation algorithm based on the background-difference method.

Suppose  $I(x, y)$  and  $B(x, y)$  are the currently obtained image and background image respectively,  $T$  is the threshold we set, and  $f(x, y)$  is the result image, then the quantum image segmentation algorithm can be described as:

$$f(x, y) = \begin{cases} 1, & |B(x, y) - I(x, y)| \geq T \\ 0, & |B(x, y) - I(x, y)| < T \end{cases} . \tag{3}$$

From the formula, we can see that a quantum absolute value subtractor and a quantum comparator are needed. The function of the quantum absolute value subtractor is to subtract

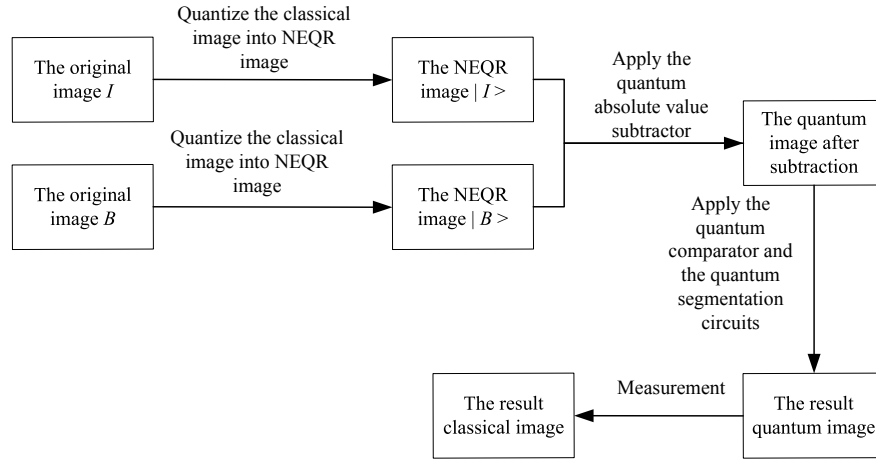


Fig. 2. Workflow of our proposed algorithm.

the current image and the background image to obtain the object gray-scale image. The function of the quantum comparator is to compare the obtained gray-scale image with the threshold, and finally obtain a binary image. Therefore, we need an eight-qubit quantum absolute subtractor and an eight-qubit quantum comparator. In this paper, a combination of a quantum comparator, eight CSWAP gates and a quantum subtractor is used to implement the absolute value subtractor. We first use the comparator to compare the two gray-scale values that need to be subtracted, and then the CSWAP gates are used to perform the swap operation, which can set the large gray-scale value as the subtracted number. In this way, the subtractor can always subtract the small qubit sequence from the large qubit sequence, so that the effect of the absolute value subtractor can be obtained. After performing the absolute value subtraction operation, we will get a gray-scale image containing the object. In order to prevent the influence of light and other factors, we set a threshold, and input the obtained gray-scale image into the comparator to compare the image's gray-scale value with the threshold, and finally we will get a binary image. From this, we can use quantum circuits to distinguish dynamic objects in stationary scenes.

### 3.2 Circuit design of the quantum segmentation algorithm

#### 3.2.1 Quantum comparator

The quantum comparator (QC) is used to compare the magnitude relationship of two quantum sequence values, and it takes two binary number sequences  $|a\rangle = |a_{n-1}a_{n-2}\cdots a_0\rangle$  and  $|b\rangle = |b_{n-1}b_{n-2}\cdots b_0\rangle$  as input and the comparison result  $y = 0$  or  $y = 1$  as output. In the quantum bit string comparator (QBSC) [33], after inputting two quantum bit strings, three relations can be obtained. If  $a > b$ , then  $x = 1$ ,  $y = 0$ , if  $a < b$ , then  $x = 0$ ,  $y = 1$ , if  $a = b$ , then  $x = y = 0$ . In this paper, an eight-qubit quantum comparator is used to compare the gray-scale value of the image, and we only need to know the two relationships  $a \geq b$  and

$a < b$ , as shown in Fig. 3.  $a_7 \cdots a_1 a_0$  and  $b_7 \cdots b_1 b_0$  represent two numbers that need to be compared, and  $h_2 h_1 h_0$  represents auxiliary qubits. We compare them one by one from the lowest bit to the highest bit. If  $a_0 = 0, b_0 = 1$ , then  $y = 1$  and the auxiliary qubit  $h_2$  is set to 1. otherwise  $y = 0$  and  $h_2$  remains unchanged. At this point, the comparison of  $a_0$  and  $b_0$  is over. The next qubits is compared according to the same comparison method as before. If the next comparison result of  $a_1$  and  $b_1$  is 1, then  $b > a$ , and  $y = 1$  is output directly and  $h_1$  is set to 1, otherwise the comparison result of the previous qubit  $a_0$  and  $b_0$  is output and  $h_1$  remains unchanged. When the two comparison results are synthesized,  $a_1 b_1 a_0 b_0 = 1001$  needs to be considered separately, so we use 2 Toffoli gates and one CNOT gate to process the two comparison results, which also requires an auxiliary qubit  $h_0$  to store the second comparison result. After the two qubits comparisons, we use two reset operations [34] to set the auxiliary qubits  $h_2 h_0$  to 0, so that we can reuse the two auxiliary qubits. According to this comparison method, we can compare the sequence of  $n$  qubits. Compared with the existing quantum comparators, and from Tab. 2, it can be seen that our comparator can operate with the fewer auxiliary qubits and the lower quantum cost, which is very meaningful in this NISQ era. The complete 8-qubit quantum subtractor circuit is shown in Fig. A.1.

Table 2. Comparison of different quantum comparators..

Quantum comparator	Auxiliary qubits	Quantum cost
QBSC[33]	$3n - 1$	$30n - 15$
QC[29]	5	$28n - 15$
our comparator	3	$18n - 13$

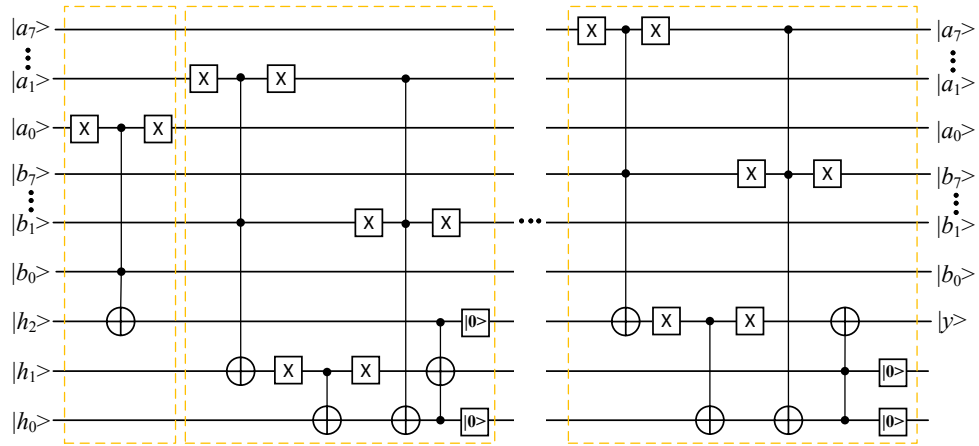


Fig. 3. 8-qubit quantum comparator implementation circuit.

### 3.2.2 Design of quantum subtractor

In the algorithm, we need to subtract one image from another, so a quantum subtractor (QS) is required. The subtractor takes two binary number sequences  $|a\rangle = |a_{n-1} a_{n-2} \cdots a_0\rangle$  and  $|b\rangle = |b_{n-1} b_{n-2} \cdots b_0\rangle$  as input, and outputs the result of  $a - b$ . According to the idea of the

ripple carry adder [35], our subtractor is also designed bit by bit from the lowest bit ( $a_0$ ) to the highest bit ( $a_{n-1}$ ). The subtraction of  $a_0 - b_0$  only needs to consider the four cases of  $0-0$ ,  $0-1$ ,  $1-0$ , and  $1-1$ . From these four cases, we can see that there is no need to perform any operation in the cases of  $0-0$  and  $1-0$ , and we directly output  $a_0$  as the subtraction result. If  $a_0 - b_0$  is  $1-1$ , then, the output result is 0. If  $a_0 - b_0$  is  $0-1$ , then, a borrow is needed from  $a_1$ . At this time, we use the Toffoli gate to mark the borrow information. From this we can see that when  $b_0$  is 1, the output result of  $a_0$  is 0. Therefore, we only need a CNOT gate operation to get the result of  $a_0 - b_0$ .

After the  $a_0 - b_0$  is completed, we use the reset operation [34] on  $b_0$ , which can reduce the consumption of qubits. The subtraction of the second bit ( $a_1 - b_1$ ) also considers whether  $a_0$  has a borrow on the basis of the subtraction of the first bit. If  $a_0$  does not borrow from  $a_1$ , then, we just follow the previous operation. If  $a_0$  has a borrow from  $a_1$ , the output result of  $1-0$  is 0 in the four cases of  $0-0$ ,  $0-1$ ,  $1-0$ , and  $1-1$ . If  $a_1 - b_1$  is  $0-0$  and  $0-1$ , then,  $a_1$  needs to borrow from  $a_2$ , and it also needs to lend a bit to  $a_0$ , so the output results are 1 and 0 respectively. If  $a_1 - b_1$  is  $1-1$ , then  $a_1$  lends a bit to  $a_0$  and then becomes 0, so it needs to borrow a bit from  $a_2$ , and the output result is 0. Therefore, we need to perform CNOT operation on the results of  $a_1 - b_1$ , and the Toffoli gates are used to record the borrow information. If  $a_1 - b_1$  is  $0-0$  or  $0-1$ , then, we write down the borrow information. If  $b_1 = 1$  and  $a_0$  needs to borrow a bit from  $a_1$ , then, we write down the borrow information. If both of these conditions exist, we also write down the borrow information. In this way, the subtraction operation of  $a_1 - b_1$  is completed, and at this time we can know whether  $a_1$  needs borrow. The subtraction operation of  $a_{n-1} - b_{n-1}$  is the same as  $a_1 - b_1$ , so, we only need to repeat the above operation to get the result of  $a_1 - b_1 \dots a_{n-2} - b_{n-2}$ . When  $a_{n-1} - b_{n-1}$ ,  $a_{n-1}$  does not need to borrow from previous bit, so we only need to consider whether  $a_{n-1}$  has a borrow.

In this paper, we presents a 8-qubit subtractor, as shown in Fig. 4.  $a_7 \dots a_1 a_0$  represent the minuend, and  $b_7 \dots b_1 b_0$  represent the subtrahend.  $h_1 h_0$  represent the auxiliary qubits, which are initialized to 0. The result of the subtraction is stored in the first 8 qubits. The subtractor designed in this paper only needs to repeat the operation of the  $a_1 - b_1$  and keep  $a_0 - b_0$  and  $a_{n-1} - b_{n-1}$  unchanged, and it can be extended to two n-qubit subtractor. The complete 8-qubit quantum subtractor circuit is shown in Fig. A.2.

### 3.2.3 *Design of quantum absolute value subtractor*

A quantum full subtractor (QFS) is designed by Cheng et al. [36] according to the classical truth tables, but it requires a large number of auxiliary qubits, which is inappropriate in this NISQ era. Thapliyal et al. [37] designed a reversible binary subtractor (RBS) based on the TR gate they proposed, but the quantum implementation of the TR gate was not known. Then, they [38] present a new design of the reversible full subtractor (RFS) based on the implementable TR gate, and the RFS is optimized in terms of quantum cost, delay and garbage outputs. But, the subtraction of two images will appear that a small gray-scale value subtracts a large value. At this time, it will generate negative numbers. But the subtractor above can only subtract small numbers from large numbers, and cannot represent negative numbers, which will cause overflow of the result. In order to prevent this case, Fan et al. [39] combines a reversible parallel subtractor (RPS) and a complement operation (CO) to form



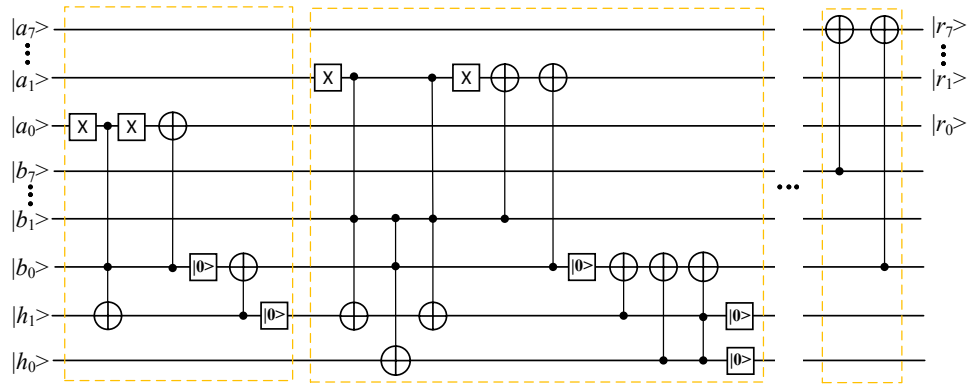


Fig. 4. 8-qubit quantum subtractor implementation circuit.

a quantum absolute value subtractor (QAVS), and its complexity is  $O(q^2)$ . This is also the most commonly used absolute value subtractor in quantum image processing [24, 39]. In this paper, we use a new method to design the absolute value subtractor to reduce the complexity of the QAVS.

First, we use the previously designed comparator to compare the two numbers that need to be subtracted. If the minuend is greater than the subtrahend, then directly input the two numbers to the subtractor, otherwise, we use the CSWAP gate to swap the position of the minuend and subtrahend. So that the minuend can be kept greater than the subtrahend, and the function of the absolute value subtractor is also achieved. Because the comparator and subtractor we designed are optimized. Therefore, the complexity of our absolute value subtractor is  $O(q)$ . Compared with the previous absolute value subtractor, the performance has been greatly improved. In this paper, we have designed a 8-qubit absolute value subtractor, as shown in Fig. 5.  $a_7 \dots a_1 a_0$  and  $b_7 \dots b_1 b_0$  represent the sequence of the minuend and the subtrahend, respectively.  $h_2 h_1 h_0$  represents the auxiliary qubits, which are initialized to 0.

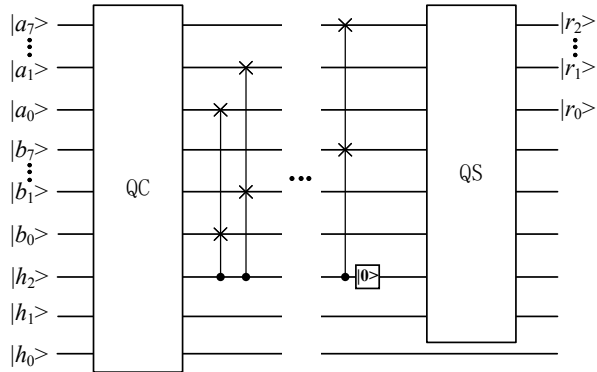


Fig. 5. 8-qubit quantum absolute value subtractor implementation circuit.

3.2.4 Design of quantum segmentation circuits

After the subtraction of the two images, we need to binarize the image after subtraction. We artificially set a threshold  $T$ , and use a quantum comparator to compare the threshold with the gray-scale value of the image. According to the comparison result, the image is converted into a binary image. When the comparison result is  $y = 0$ , it means that the gray-scale values are greater than or equal to the threshold, then we use the segmentation circuit to segment these pixels into 1. Otherwise the pixels are segmented into 0. As shown in Fig. 6,  $a_7 \dots a_1 a_0$  represent the gray-scale value,  $b_7 \dots b_1 b_0$  represent the threshold we set, and  $y$  represents the comparison result. When performing segmentation, we use a combination of CNOT gate and Toffoli gate. If  $a_n = 0$ , then we use Toffoli gate to turn it into 1, otherwise, we do not perform any operation. Through this operation, pixels greater than or equal to the threshold can be set to 1. For pixels smaller than the threshold, if  $a_n = 1$ , we use Toffoli gate to turn it into 0. The complete segmentation circuit is shown in Fig. 7.

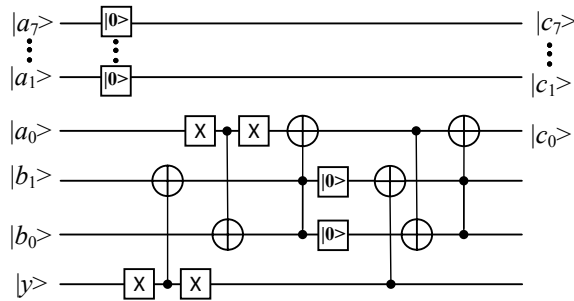


Fig. 6. 8-qubit quantum image segmentation implementation circuit S.

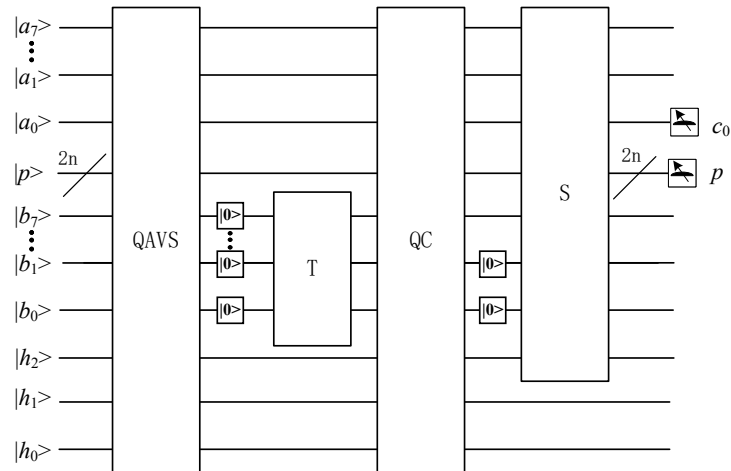


Fig. 7. The complete circuit of quantum image segmentation.

#### 4 Circuit complexity analysis

Single-qubit and double-qubit gates are the basic quantum logic gates of quantum computing and can operate on any qubit. Therefore, in this paper, we use the number of single-qubit gates and double-qubit gates to evaluate the complexity of the algorithm, which is also known as quantum cost. The quantum cost of the NOT gate and the CNOT gate is 1, and the Toffoli gate can be split into 5 double-qubit gates [40, 41, 42]. Therefore, its quantum cost is 5. In this paper, we analyze the complexity of the algorithm based on Fig. 7. Suppose the size of the image is  $2^n \times 2^n$ , and the gray-scale level is  $[0, 2^q - 1]$ . The quantum cost analysis is as follows.

As shown in Fig. 3, the design of a  $q$ -qubit quantum comparator is divided into two parts. The first part of the design requires a Toffoli gate, and the quantum cost is 5. The second part requires  $3(q - 1)$  Toffoli gates,  $(q - 1)$  CNOT gate, and  $2(q - 1)$  reset gate, so the quantum cost of the second part is  $18(q - 1)$ . Therefore, the quantum cost of a quantum comparator is  $18q - 13$ .

The design of a  $q$ -qubit quantum subtractor can be divided into three parts. The first part is the design of  $a_0 - b_0$  and we need a Toffoli gate, two CNOT gates and two reset gates. Therefore, the quantum cost of this part is 9. The second part is the design from  $a_1 - b_1$  to  $a_{q-2} - b_{q-2}$  and we need  $4(q - 2)$  Toffoli gates,  $4(q - 2)$  CNOT gates, and  $3(q - 2)$  reset gates. Therefore, the quantum cost of this part is  $27(q - 2)$ . The third part is the design of  $a_{q-1} - b_{q-1}$  and it requires 2 CNOT gates. So, the quantum cost is 2. Therefore, the quantum cost of a quantum subtractor is  $27q - 43$ .

The quantum absolute value subtractor is constructed by  $q$  CSWAP gates, a reset gate, a quantum comparator and a quantum subtractor. The quantum cost of a CSWAP gate is 3. Therefore, the quantum cost of quantum absolute value subtractor is  $48q - 55$ .

The quantum segmentation circuit is divided into two parts, and each part of the circuit is composed of a control operation and segmentation operations. The control operations are 2 CNOT gates, and the segmentation operations are composed of 2 CNOT gates, 2 Toffoli gates and  $q$  reset gates. Therefore, the quantum cost of the quantum segmentation circuit is  $q + 15$ .

The quantum circuit of our algorithm is composed of a quantum absolute value subtractor, a quantum comparator, a quantum segmentation circuit and  $q+2$  reset gates, and typically, the quantum image preparation and measurement processes are not considered part of quantum image processing [39, 24]. Therefore, the quantum cost of the algorithm is  $68q - 52$ , and the circuit complexity is  $O(q)$ . The detailed quantum cost of each quantum circuit unit is shown in Tab. 3. This shows that the complexity of our algorithm is only related to the gray-scale level of the image, and has nothing to do with the size of the image. Since the classic image segmentation algorithm needs to process each pixel in turn, the algorithm complexity is not lower than  $O(2^{2n})$  [43, 44]. Therefore, our algorithm can achieve exponential acceleration compared to classic algorithms. The algorithm our proposed is compared with some other classical and quantum image segmentation algorithms in references [44, 26, 27, 29]. For convenience, the segmentation algorithms in [44, 26, 27, 29] are abbreviated as BSMOG, IS, NMQCIS, DQIS, respectively. The detailed information is shown in Tab. 4.

It can be seen from Tab. 4 that  $3q-1$  auxiliary qubits are used to segment the quantum

Table 3. The quantum cost and complexity of different quantum circuit unit.

Unit	Quantum cost	Complexity
Quantum comparator	$18q - 13$	$O(q)$
Quantum subtractor	$27q - 43$	$O(q)$
Absolute value subtractor	$48q - 55$	$O(q)$
Binaryzation	$q + 15$	$O(q)$

Table 4. Comparison of the different segmentation algorithms.

Algorithms	Object state	Auxiliary qubits	quantum cost	Complexity
BSMOG[44]	dynamic	-	-	$O(2^{2n})$
IS [26]	static	$3q-1$	$127q-91$	$O(q)$
NMQCIS [27]	static	18	$48q-6$	$O(q)$
DQIS [29]	static	5	$70q-14$	$O(q)$
Our algorithm	dynamic	3	$68q-52$	$O(q)$

image into a binary image in IS algorithm. It uses two  $q$ -qubit QBSCs to distinguish the relationships between the gray-scale values and the threshold, and the quantum cost of 1-qubit QBSC is 14. So, the quantum cost of IS algorithm is  $127q - 91$ . In the NMQCIS algorithm, 18 auxiliary qubits and one half-comparator are used to segment the quantum image into a binary image. In addition,  $2q$  swap gates with 3 control qubits are used for image segmentation. The quantum cost of the algorithm is  $48q-6$ . In the DQIS algorithm, two thresholds and two comparators are used to segment the quantum image, which require 5 auxiliary qubits. Moreover, the quantum cost of one quantum comparator is  $28q-15$ . Additional  $2q+2$  Toffoli gates,  $2q$  CNOT gates, 4 NOT gates and  $2q+2$  reset gates are used to compose the complete circuit. When evaluating the quantum cost, only one quantum comparator's quantum cost is considered, and the quantum cost is  $42q+1$ . However, under normal circumstances, we should calculate each operation that is used. So, the quantum cost of DQIS algorithm is  $70q-14$ . In addition, the pixels greater than the high threshold and smaller than the low threshold are segmented into 0, and the other pixels remain unchanged, which is inappropriate for complex images. The above quantum segmentation algorithms can only segment static objects in static scene images, and their complexity is  $O(q)$ .

Our algorithm needs 3 auxiliary qubits, one quantum absolute value subtractor, one quantum comparator and one quantum segmentation circuit to segment dynamic objects in static scene images. Since the quantum cost of our algorithm is  $68q-52$ , the complexity is  $O(q)$ , which is the same as other quantum segmentation algorithms.

## 5 Experiment

### 5.1 Experiment preparation

At present, the IBM Q cloud platform provides some quantum computers and quantum computer simulators, but due to some factors, the number of qubits in the real quantum computer for our use is only 5 qubits, which is far from enough. Therefore, we choose a quantum computer simulator called 'ibmq\_qasm\_simulator' to perform simulation experiments through Qiskit extension [31]. This simulator has 32 qubits and can run all the basic logic

gates included in our circuit. So in this paper, all quantum circuits have been simulated and verified on this simulator. On the premise of not affecting the experimental results, for the convenience of the experiment, we select two images with a size of  $4 \times 4$  and a gray-scale range of  $[0, 255]$  for experimentation, as shown in Fig. 8. The X-axis and Y-axis indicate the position information of the pixels, and the decimal numbers indicate the gray-scale value information of each pixel. Since the NEQR model uses quantum entanglement characteristics to entangle the position information and gray-scale value information of the image to represent the quantum image, we need 10 qubits to store the gray-scale values of two images and 4 qubits to store the position information. Since the IBM Q platform initializes all qubits to  $|0\rangle$ , we use the H gate to turn  $|0\rangle$  into a superposition state of  $|0\rangle$  and  $|1\rangle$ , so that four qubits can be used to represent all the position information of the  $4 \times 4$  image. In addition, we use basic quantum logic gate operations to entangle position information and gray-scale value information. In this way, we can prepare the NEQR images. Since the threshold is a definite value, we only need to set it using the NOT gate, and in this experiment, the threshold was set to 104.

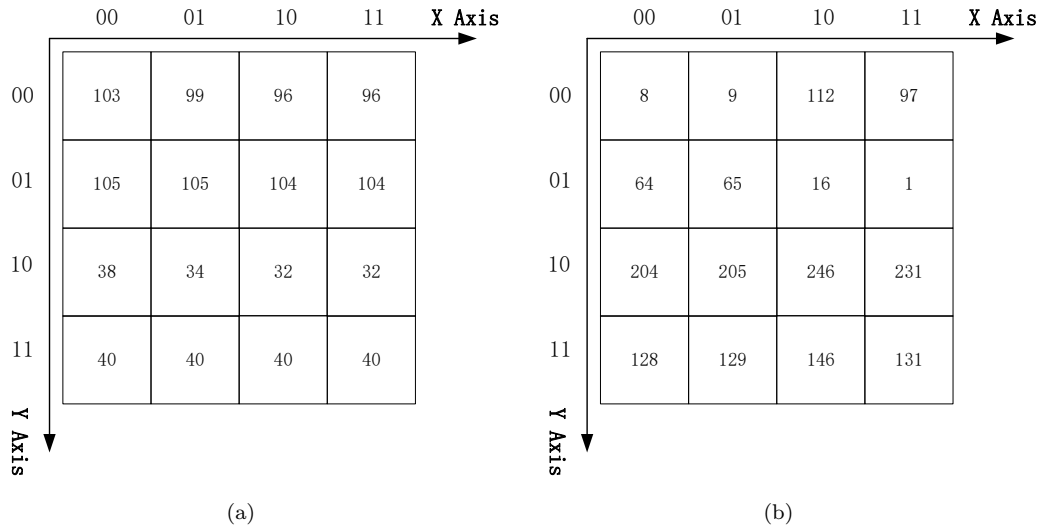


Fig. 8. Schematic diagram of the original quantum image. ( Suppose a and b are images of the same scene at different moments.)

### 5.2 Result analysis

Fig. 9 is the probability histogram of the result image, and the number of measurement is 1024. From the probability histogram, it can be seen that the probability amplitudes of the measured quantum sequences are different, which further validates the randomness and uncertainty principles of the quantum system. The binary sequences below the probability histogram is the measured qubits sequences, which are arranged in order from top to bottom. The gray-scale values and the position information of the result image are marked in Fig. 9, where C represents the gray-scale value and P represents the position. Other qubits form a complete circuit, and we don't pay attention to their output results. The experimental result shows the feasibility of our algorithm. Fig. 10 is the result image, and the position

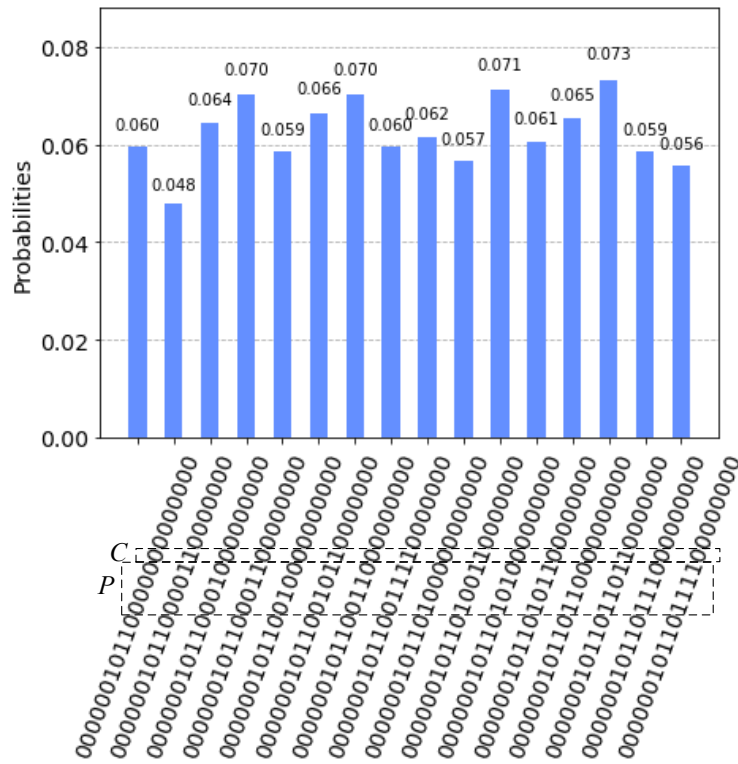


Fig. 9. Probability histogram of the resulting quantum image.

information and the gray-scale value information have been marked in it. As can be seen from the result image, our algorithm can effectively segment gray-scale images.

## 6 Conclusion

The existing quantum image segmentation algorithms can only segment static objects, and since they use too many quantum cost and qubits, they are not applicable in this NISQ era. In this paper, a novel quantum image segmentation algorithm based on the background-difference method for NEQR image is proposed, which can segment dynamic objects from static scene images by using less quantum cost and qubits. In addition, a feasible quantum absolute value subtractor is designed, which has an exponential performance improvement compared with the existing quantum absolute value subtractor. Then, we design a complete quantum image segmentation circuit that can segment quantum images by using fewer qubits. The circuit complexity analysis and experiment on IBM Q platform show the superiority and feasibility of our proposed algorithm.

However, our algorithm is only suitable for image segmentation with a constant background, which is less effective for image segmentation with changing backgrounds. Therefore, our future work is to further optimize the algorithm and apply it to image segmentation with changing backgrounds.

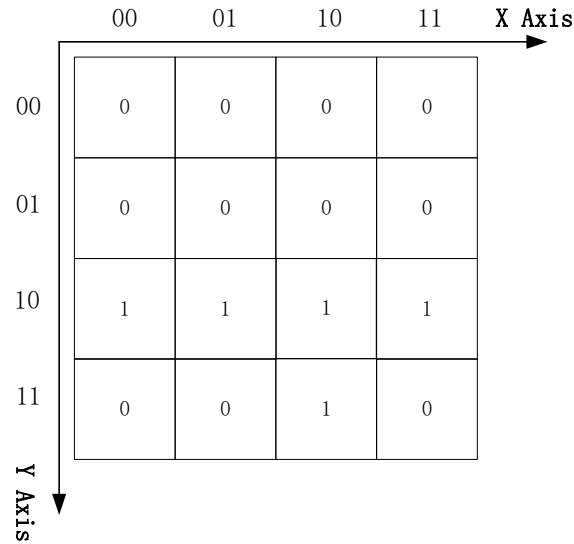


Fig. 10. Schematic diagram of the result quantum image.

### Acknowledgements

This work is supported by the National Natural Science Foundation of China (62071240), the Innovation Program for Quantum Science and Technology (2021ZD0302901), and the Priority Academic Program Development of Jiangsu Higher Education Institutions (PAPD).

### References

1. F. Yan, A. M. Ilyasu and P. Q. Le (2017), *Quantum image processing: A review of advances in its security technologies*, International Journal of Quantum Information, Vol. 15, no. 3, 1730001.
2. Y. Cai, L. U. Xiao and N. Jiang (2018), *A survey on quantum image processing*, Chinese Journal of Electronics, Vol. 27, no. 4, pp. 56-65.
3. S. E. Venegas-Andraca and S. Bose (2003), *Storing, processing, and retrieving an image using quantum mechanics. Proceedings of the SPIE Conference on Quantum Information and Computation*, pp. 137-147.
4. J. I. Latorre (2005), *Image compression and entanglement*, arXiv:quant-ph/0510031
5. P. Q. Le, F. Dong, and K. Hirota (2011), *A flexible representation of quantum images for polynomial preparation*, Quantum Inf. Process., Vol. 10, no. 1, pp. 63-84.
6. B. Sun, A. M. Ilyasu, F. Yan, F. Dong, and K. Hirota (2013), *An RGB multi-channel representation for images on quantum computers*, Adv. Comput. Intell. Inform. vol. 17, no.3, pp. 404-417.
7. H. S. Li, Q. Zhu, R. G. Zhou, et.al (2014), *Multi-dimensional color image storage and retrieval for a normal arbitrary quantum superposition state*, Quantum inf. Process. vol. 13, no. 4, pp. 991-1011.
8. X. W. Yao, H. Wang, Z. Liao, M. C. Chen, J. Pan, J. Li, et.al (2018), *Quantum Image Processing and Its Application to Edge Detection: Theory and Experiment*, arXiv:quant-ph/1801.01465
9. Y. Zhang, L. Kai, Y. Gao and M. wang (2013), *NEQR: a novel enhanced quantum representation of digital images*, Quantum Inf. Process., Vol. 12, no. 8, pp. 2833-2860.
10. N. Jiang and L. Wang (2015) *Quantum image scaling using nearest neighbor interpolation*, Quantum Inf. Process., Vol. 14, no. 5, pp. 1559-1571.
11. Y. Zhang, K. Lu, K. Xu, Y. Gao and R. Wilsion (2015) *Local feature point extraction for quantum*

- images*, Quantum Inf. Process., Vol. 14, no. 5, pp. 1573–1588.
12. J. Sang, S. Wang, and Q. Li, (2017), *A novel quantum representation of color digital images*, Quantum Information Processing, Vol. 16, no. 2, pp. 42.
  13. E. Sahin and I. Yilmaz (2018), *QRMW: quantum representation of multi wavelength images*, TURKISH JOURNAL OF ELECTRICAL ENGINEERING AND COMPUTER SCIENCES, Vol. 26, no. 2, pp. 768-779.
  14. R. G. Zhou, C. Tan and H. Lan (2017), *Global and local translation designs of quantum image based on FRQI*, International Journal of Theoretical Physics, Vol. 56, no. 4, pp. 1-17.
  15. R. G. Zhou, Q. Wu, M. Q. Zhang and C. Y. Shen (2013), *Quantum image encryption and decryption algorithms based on quantum image geometric transformations*, International Journal of Theoretical Physics, Vol. 52, no. 6, pp. 1802-1817.
  16. E. R. Hancock (2015), *Local feature point extraction for quantum images*, Quantum Inf. Process., Vol. 14, no. 5, pp. 1573-1588.
  17. R. G. Zhou (2015), *Quantum image gray-code and bit-plane scrambling*, Quantum Inf. Process., Vol. 14, no. 5, pp. 1717–1734.
  18. S. Yuan, X. Mao, T. Li, Y. Xue, L. Chen and Q. Xiong (2015), *Quantum morphology operations based on quantum representation model*, Quantum Inf. Process., Vol. 14, no. 5, pp. 1625–1645.
  19. R. G. Zhou, W. Hu, P. Fan and G. Luo (2018), *Quantum color image watermarking based on arnold transformation and lsb steganography*, Int. J. Quantum Inf., Vol. 3, no. 16, 1850021.
  20. P. Li, X. Liu and X. Hong (2017), *Quantum image weighted average filtering in spatial domain*, International Journal of Theoretical Physics, Vol. 56, no. 11, pp. 1-27.
  21. Y. Zhang, K. Lu and Y. H. Gao (2015), *A novel quantum image edge extraction algorithm*, Science China Information Sciences, Vol. 58, no. 1, pp. 12106–012106.
  22. R. G. Zhou and D. Q. Liu (2019), *Quantum image edge extraction based on improved sobel operator*, International Journal of Theoretical Physics, Vol. 58, no. 9, pp. 1–17.
  23. P. Fan, R. G. Zhou, W. W. Hu and N. Jing (2015), *Quantum image edge extraction based on classical sobel operator for NEQR*, Quantum Inf. Process., Vol. 18, no. 1, 24.
  24. R. Chetia, S. Boruah and P. P. Sahu (2021), *Quantum image edge detection using improved sobel mask based on NEQR*, Quantum Inf. Process., Vol. 20, no. 1, 21.
  25. S. Caraiman and V. I. Manta (2014), *Histogram-based segmentation of quantum images*, Theoretical Computer Science, Vol. 529, no. 6, pp. 46–60.
  26. S. Caraiman and V. I. Manta (2015), *Image segmentation on a quantum computer*, Quantum Inf. Process., Vol. 14, no. 5, pp. 1693–1715.
  27. H. Xia, H. Li, H. Zhang, Y. Liang and J. Xin (2019), *Novel multi-bit quantum comparators and their application in image binarization*, Quantum Inf. Process., Vol. 18, no. 7, 229.
  28. A. Youssry, E. Ahmed and E. Salwa (2015), *A quantum mechanics-based framework for image processing and its application to image segmentation*, Quantum Inf. Process., Vol. 14, no. 10, pp. 3613-3638.
  29. S. Yuan, C. Wen, B. Hang and Y. Gong (2020), *The dual-threshold quantum image segmentation algorithm and its simulation*, Quantum Inf. Process., Vol. 19, no. 12, 425.
  30. IBM Quantum Lab (2022), *IBM Q*, <https://www.research.ibm.com/ibm-q/>.
  31. G. Aleksandrowicz, T. Alexander, P. Barkoutsos, L. Bello and Y. Ben-Haim (2019), *Qiskit: an open-source framework for quantum computing*.
  32. M. A. Nielsen and I. L. Chuang (2000), *Quantum computation and quantum information*, Academic Press (Cambridge University).
  33. R.V. Oliveira and D.S. Ramos (2007), *Quantum bit string comparator: Circuits and applications. quantum computers and computing*, Quantum Inf. Comput., Vol. 7, no. 1, pp. 17–26.
  34. V.V. Shende, S.S. Bullock and I.L. Markov (2005), *Synthesis of quantum logic circuits*, Proceedings of the 2005 Asia and South Pacific Design Automation Conference, vol. 4, pp. 272–275.
  35. H. Thapliyal and N. Ranganathan (2013), *Design of efficient reversible logic-based binary and bcd adder circuits*, J. Emerg. Technol. Comput. Syst., Vol. 9, no. 3, pp. 1-31.
  36. K.W. Cheng and C.C. Tseng (2002), *Quantum full adder and subtractor*, Electron. Lett., Vol. 38,



- no. 22, pp. 1343–1344.
37. H. Thapliyal and N. Ranganathan (2009), *Design of efficient reversible binary subtractors based on a new reversible gate*, 2009 IEEE Computer Society Annual Symposium on VLSI, IEEE, pp. 229–234.
  38. H. Thapliyal and N. Ranganathan (2009), *A new design of the reversible subtractor circuit*, 2011 11th IEEE International Conference on Nanotechnology, IEEE, pp. 1430–1435.
  39. P. Fan, R.G. Zhou, W.W. Hu and N. Jing (2019), *Quantum image edge extraction based on Laplacian operator and zero-cross method*, Quantum Inf. Process. vol. 18, no. 1, 27.
  40. H.S. Li, P. Fan, H.Y. Xia, H.L. Peng and G.L. Long (2020), *Efficient quantum arithmetic operation circuits for quantum image processing*, Science China Physics, Mechanics & Astronomy, vol. 63, no. 8, 280311.
  41. T. Sleator and H. Weinfurter (1995), *Realizable universal quantum logic gates*, Physical Review Letters, vol. 74, no. 20, 4087.
  42. M. A. NIELSEN and I. L. CHUANG(2000), *Quantum information theory*, Cambridge: Cambridge University Press.
  43. N. McFarlane and C. Schofield (1995), *Segmentation and tracking of piglets in images*, Machine Vision Applications, vol. 8, no. 3, pp. 187-193.
  44. Z. Zivkovic(2004), *Improved adaptive Gaussian mixture model for background subtraction*, Proceedings of the 17th International Conference on Pattern Recognition, IEEE, pp. 28-31.

## Appendix A

Fig.A.1 and Fig.A.2 are the complete 8-qubit quantum circuit of the comparator and the subtractor.

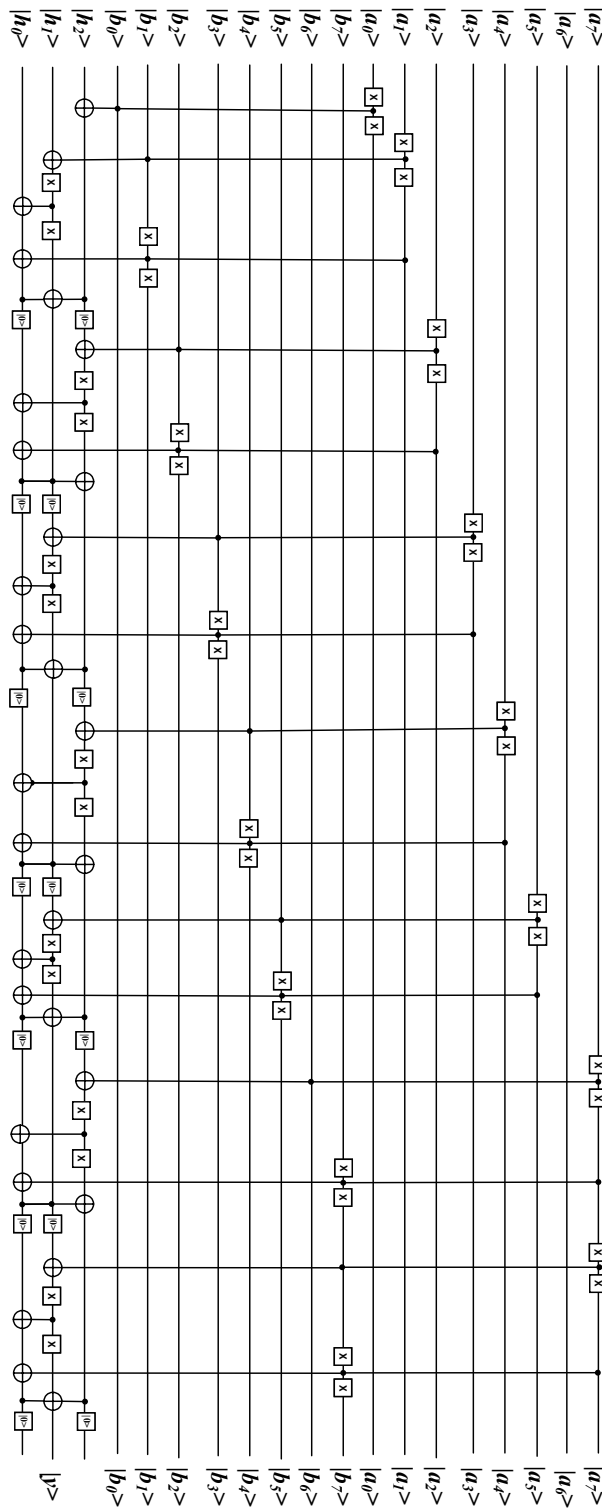


Fig. A.1.  
The complete 8-qubit quantum comparator.

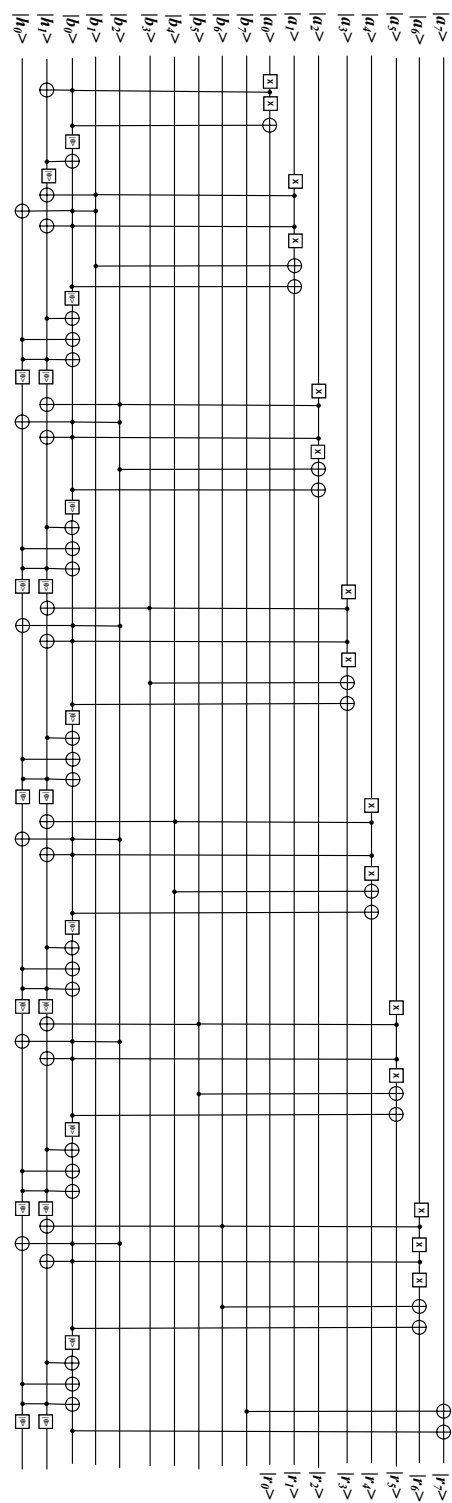


Fig. A.2.  
The complete 8-qubit quantum subtractor.